Magma oxygen fugacity of mafic-ultramafic intrusions in convergent margin settings: insights for the role of magma oxidation states on magmatic Ni-Cu sulfide mineralization

Yonghua Cao [1, 2], Christina Yan Wang [1, 2]*, Bo Wei [1, 2]

[1] CAS Key Laboratory of Mineralogy and Metallogeny, Guangzhou Institute of Geochemistry, Chinese Academy of Sciences, Guangzhou 510640, China

[2] Guangdong Provincial Key Laboratory of Mineral Physics and Materials, Guangzhou 510640, China

Corresponding author: Dr. C.Y. Wang (wang_yan@gig.ac.cn)

Supplementary Information

1. Mafic-ultramafic intrusions in the CAOB selected to calculate magma fO_2

The ca. 430 Ma Jinbulake intrusion in the Central Tianshan belt is a concentric body and consists of wehrlite in the inner core and olivine gabbro and gabbro in the outer shell (Yang et al., 2012). Fourteen wehrlite samples from the open pit consist mainly of cumulus olivine and clinopyroxene (Fig. S1a). Fine-grained spinel (1 to 2 modal%) is commonly enclosed within or interstitial to olivine. Minor amounts of plagioclase occupy the interstices between olivine and clinopyroxene. The rocks contain ~1 modal% sulfides.

The ca. 356 to 367 Ma Heishan intrusion in the Beishan belt consists mainly of

American Mineralogist: December 2020 Deposit AM-20-127351

harzburgite and lherzolite (Xie et al., 2012). The rocks are mainly composed of cumulus olivine and orthopyroxene. Clinopyroxene and plagioclase are present in the interstices between olivine and orthopyroxene. Spinel (~1 modal%) is commonly enclosed within the olivine of lherzolite and harzburgite. In this study, we analyzed the composition of the olivine from the same suite of the samples reported in Xie et al. (2012).

The ca. 294 Ma Erbutu intrusion in the Xing'an-Mongolia belt consists mainly of olivine orthopyroxenite. Fourteen samples from the open pit mainly contain cumulus orthopyroxene and olivine, with minor amounts of clinopyroxene, hornblende and plagioclase as interstitial phases (Fig. S1b). Fine-grained spinel (1 to 2 modal%) is commonly enclosed within olivine. Sulfides (<5 modal%) are disseminated in the rocks.

The ca. 286 Ma Baixintan intrusion in the North Tianshan belt consists of lherzolite, olivine websterite, olivine norite and gabbro (Feng et al., 2018). Spinel is only observed in lherzolite. Four drill-core samples of lherzolite are mainly composed of cumulus olivine and/or orthopyroxene, with clinopyroxene and plagioclase as the main interstitial phases (Fig. S1c). Fine- to medium-grained spinel (1 to 2 modal%) is mainly enclosed within olivine. The rocks contain ~1 modal% sulfides. Some chemical data of the olivine-spinel pairs in lherzolite samples were collected from the literature (*c.f.*, Feng et al., 2017, 2018).

The ca. 278 Ma Huangshannan intrusion in the North Tianshan belt consists of lherzolite, olivine websterite and gabbronorite (Mao et al., 2016). Thirteen lherzolite samples from drill cores are composed of cumulus olivine and/or orthopyroxene, with interstitial clinopyroxene and hornblende (Fig. S1d). Fine- to medium-grained spinel

(<5 modal%) is either enclosed within olivine or interstitial to olivine. The samples contain <5 modal% sulfides.

The ca. 260-290 Ma Luodong intrusion in the Beishan belt consists mainly of dunite, olivine pyroxenite and gabbro (Su et al., 2011). Seven dunite samples from the open pit are mainly composed of cumulus olivine, with minor amounts of clinopyroxene and/or orthopyroxene as interstitial phases (Fig. S1e). The rocks contain <1 modal% sulfides. Some chemical data of olivine-spinel pairs in dunite are collected from Su et al. (2011).

The ca. 265 Ma Tulaergen intrusion in the North Tianshan belt consists of lherzolite, hornblende (olivine) websterite and hornblende gabbro (Zhao et al., 2017). Six lherzolite samples from the open pit are mainly composed of cumulus olivine and orthopyroxene, with interstitial clinopyroxene and plagioclase (Fig. S1f). Fine- to medium-grained spinel (<5 modal%) is mainly enclosed within olivine. The rocks contain disseminated to semi-massive sulfides.

The Dali picrite is part of the ca. 260 Ma Emeishan large igneous province (LIP) that occurs in the southwestern margin of the Yangtze Block (Chung and Jahn, 1995; Xu et al., 2001). The Dali picrite has OIB-like trace element patterns (*e.g.*, Wu et al., 2018), representative of the primitive magma compositions of the mafic-ultramafic intrusions in the Emeishan LIP (*e.g.*, Hanski et al., 2010). The picrite contains abundant euhedral olivine phenocrysts, and fine- to medium-grained spinel that is commonly enclosed within the olivine (Kamenetsky et al., 2012; Liu et al., 2017). The compositions of olivine-spinel pairs in the picrite were collected from the literature (*c.f.*, Kamenetsky et al., 2012; Liu et al., 2017).

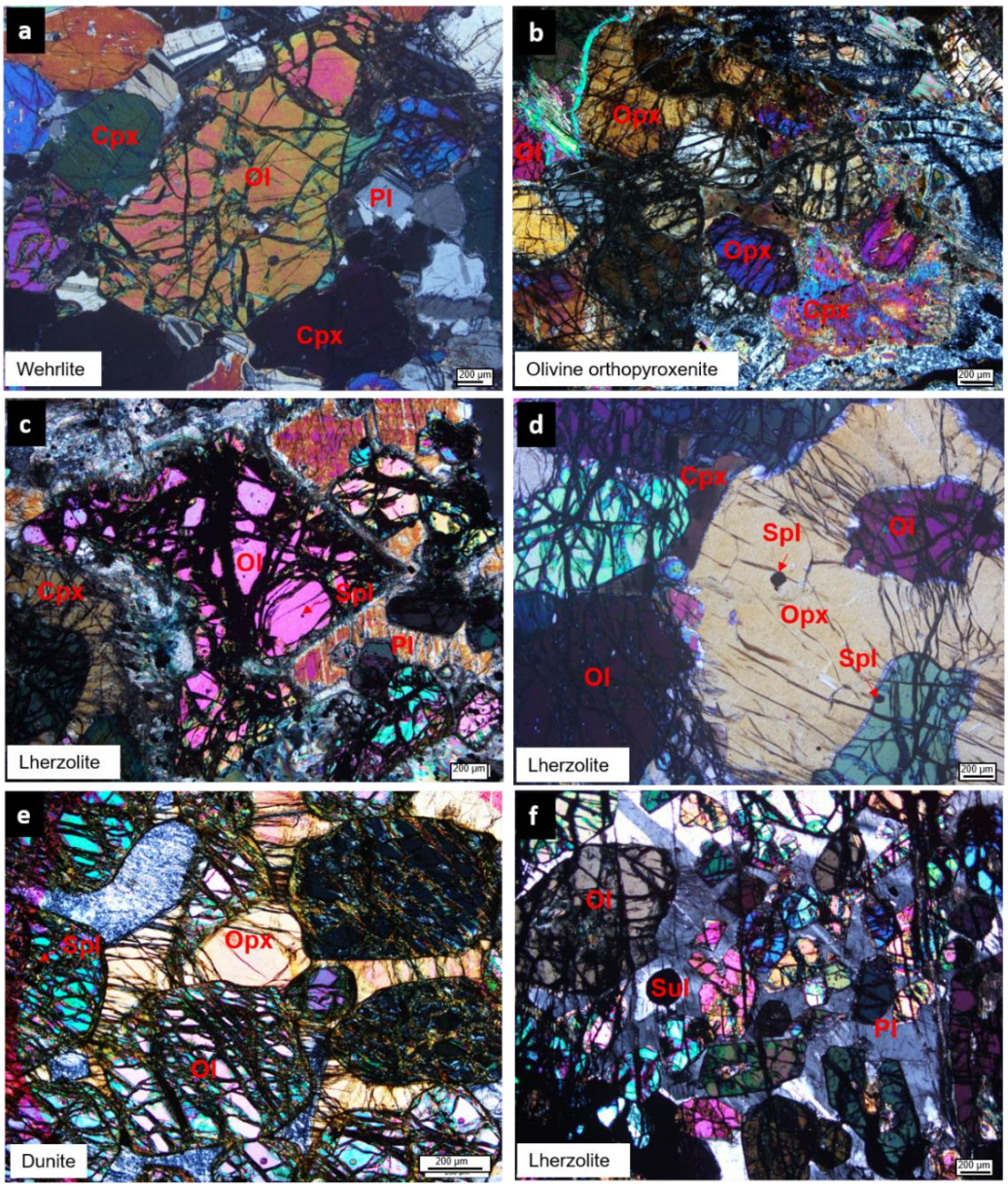

Fig. S1. Photomicrographs of representative ultramafic rock samples from (a) the Jinbulake intrusion, (b) the Erbutu intrusion, (c) the Baixintan intrusion, (d) the Huangshannan intrusion, (e) the Luodong intrusion, (f) the Tulaergen intrusion.
Abbreviations: Cpx-clinopyroxene, Ol-olivine, Opx-orthopyroxene, Pl-plagioclase, Spl-spinel, Sul-sulfides.

2. Analytical methods

2.1 *Major elements of olivine and spinel*

Major element compositions of olivine and spinel were determined by electron probe microanalyzer (EPMA) JEOL JXA-8230 at the CAS Key Laboratory of

Mineralogy and Metallogeny. Polished thin sections were carbon coated. Operating conditions were 15 kV, 20 nA and a 1 μm beam for all analyzed elements. Peak and background counting times are: (1) 20 and 10 s, respectively, for Si, Fe and Mg; 40 and 20 s, respectively, for Ti and Mn; and 60 and 30 s, respectively, for Cr, Ni, when analyzing olivine, and (2) 20 and 10 s, respectively, for Si, Al, Fe, Mg and Ca; 40 and 20 s, respectively, for Ti and Mn; and 60 and 30 s, respectively, for Cr and Ni, when analyzing spinel. The standards used were olivine for Si and Mg, magnetite for Fe, Ni metal for Ni, diopside for Ca, rhodonite for Mn, almandine garnet for Al, Cr_2O_3 metal for Cr, and rutile for Ti. Detection limits for analyzed elements are typically less than ~100 ppm and no peak overlapping corrections are needed. Analytical results were reduced using the ZAF correction routines.

The Fe^{3+} and Fe^{2+} contents of spinel were calculated by assuming perfect stoichiometry (*c.f.*, Droop, 1987), which were then corrected using a set of spinel standards (BAR8601-9, BAR8601-10, DB8803-3, IM8703, KLB8320, MHP79-4, Mo103, Mo4230-16, and Vi86-1) following the method proposed by Davis et al. (2017). Details about this correction were given in Cao et al. (2019).

2.2 *Trace elements of olivine*

Trace element compositions of olivine were analyzed using a laser ablation inductively coupled-plasma spectrometry (LA-ICP-MS) at the CAS Key Laboratory of Mineralogy and Metallogeny. The Agilent 7500a ICP-MS instrument was coupled to a Resonitics 193 nm ArF laser ablation system. The beam size for a single spot ablation is 31 μm. Laser energy was 80 mJ and ablation frequency was 6 Hz. Helium gas was

used as a carrier gas. NIST SRM 610 glass was employed as an external standard and GOR-132 glass was treated as an unknown sample. The MgO content of olivine determined by EPMA was used as an internal standard. Data reduction was performed using the ICPMSDataCal software (version 10.2) (Liu et al., 2008). The detection limit is ~0.06 ppm for V and ~0.1 ppm for Sc, and the analytical uncertainty is better than 10% (relative) for both elements. The measured V and Sc concentrations of NIST SRM 610 and GOR-132 and their recommended values are listed in the table below.

Table. Measured trace element concentrations of NIST SRM 610 and GOR-132

	NIST SRM 610		GOR-132		
Elements	Recommended (ppm ± 1 σ)	Measured (*n*=20) (ppm ± 1 σ)	Recommended (ppm ± 1 σ)	Measured (*n*=20) (ppm ± 1 σ)	Detection limit (ppm)
V	450±10	474±1	202±20	218±2	0.06
Sc	455±20	502±2	35.6±1.4	37.3±0.4	0.1

Note: The recommended values of NIST SRM 610 and GOR-132 are from Jochum et al. (2011) and Jochum et al. (2006), respectively.

2.3 *S isotope of sulfides*

In situ S isotope analysis for sulfide minerals (pyrrhotite, pentlandite and chalcopyrite) were performed using a Nu Plasma 1700 HR multicollector inductively coupled plasma-mass spectrometer (MC-ICP-MS) equipped with a Resonitics 193 nm excimer ArF laser ablation system at the State Key laboratory of Continental Dynamics, Northwest University. Samples were ablated within a HelEx ablation cell using He gas, with gas flows at 0.86 L/min. The S isotopes of sulfides were analyzed at medium resolution. During ablation, the data were collected in static mode (^{32}S, ^{33}S and ^{34}S). S isotopic compositions of pyrrhotite and pentlandite grains were calibrated using a pyrite

standard (Py-4: $\delta^{34}S_{V\text{-}CDT}$=1.7±0.3‰, 2SD), and those of chalcopyrite grains were calibrated using a chalcopyrite standard (Cpy-1: $\delta^{34}S_{V\text{-}CDT}$=4.2±0.3‰, 2SD). The total S signal obtained for pyrite and chalcopyrite standards was 10 V and 2 V, respectively. The integration time was 20 s for baseline and 30 to 40 s for ablation. Detailed analytical methods and procedures can be referred to Chen et al. (2017), Bao et al. (2017) and Yuan et al. (2018).

3. Compositions of olivine-spinel pairs in mafic-ultramafic intrusions in the CAOB and the Dali picrite

3.1 *Silurian to Carboniferous mafic-ultramafic intrusions in the CAOB*

Olivine grains in the wehrlite of the Jinbulake intrusion have Fo contents [molar 100Mg/(Mg+Fe^{2+})] ranging from 83 to 86 (Table S2). The grains in the lherzolite and harzburgite of the Heishan intrusion have Fo contents ranging from 82 to 87 (Wang, 2011). The grains in the olivine orthopyroxenite of the Erbutu intrusion have Fo contents ranging from 83 to 86 (Table S2).

Spinel grains in the wehrlite of the Jinbulake intrusion have Cr_2O_3 varying from 15 to 30 wt.% and Al_2O_3 from 30 to 45 wt.%, with Cr# [molar 100Cr/(Cr+Al)] ranging from 18 to 59 (Table S2). They have Mg# [molar 100Mg/(Mg+Fe^{2+})] varying from 20 to 46, and XFe^{3+} [molar Fe^{3+}/(Fe^{3+}+Cr+Al)] ranging from 0.04 to 0.17. Spinel grains in the lherzolite and harzburgite of the Heishan intrusion have Cr_2O_3 varying from 31 to 37 wt.% and Al_2O_3 from 16 to 23 wt.%, with Cr# ranging from 51 to 61 (Table S2). They have Mg# varying from 32 to 49 and XFe^{3+} from 0.11 to 0.18. Spinel grains in the olivine orthopyroxenite of the Erbutu intrusion have Cr_2O_3 varying from 31 to 50

wt.% and Al_2O_3 from 10 to 33 wt.%, with Cr# ranging from 49 to 70 (Table S2). They have Mg# varying from 24 to 47 and XFe^{3+} from 0.03 to 0.09.

The Mg/Fe distribution coefficient of equilibrated olivine-spinel pairs is expressed as $Kd_{Mg/Fe}^{Ol-Spl}$ [molar $(Mg/Fe^{2+})_{Ol}/(Mg/Fe^{2+})_{Spl}$]. The calculated $Kd_{Mg/Fe}^{Ol-Spl}$ for the samples from the Jinbulake, Heishan and Erbutu intrusions ranges from 5.7 to 10.5, 5.7 to 11.0, and 6.9 to 17.9, respectively (Table S2).

3.2 *Permian to Triassic mafic-ultramafic intrusions in the CAOB*

Olivine grains in the lherzolite of the Baixintan, Huangshannan and Tulaergen intrusions have Fo contents ranging from 82 to 86, 81 to 87, and 81 to 85, respectively (Table S2). Olivine grains in the dunite of the Luodong intrusion have Fo contents ranging from 85 to 89 (Table S2).

Spinel grains in the lherzolite of the Baixintan intrusion have Cr_2O_3 varying from 11 to 34 wt.% and Al_2O_3 from 6 to 23 wt.%, with Cr# ranging from 50 to 75. They have Mg# varying from 6 to 56 and XFe^{3+} from 0.10 to 0.50 (Table S2). Spinel grains in the lherzolite of the Huangshannan intrusion have Cr_2O_3 varying from 31 to 44 wt.% and Al_2O_3 from 17 to 44 wt.%, with Cr# ranging from 39 to 76. They have Mg# varying from 11 to 40 and XFe^{3+} from 0.03 to 0.22 (Table S2). Spinel grains in the dunite of the Luodong intrusion have Cr_2O_3 varying from 26 to 34 wt.% and Al_2O_3 from 26 to 42 wt.%, with Cr# ranging from 34 to 47. They have Mg# varying from 28 to 50 and XFe^{3+} from 0.05 to 0.09 (Table S2). Spinel grains in the lherzolite of the Tulaergen intrusion have Cr_2O_3 varying from 28 to 34 wt.% and Al_2O_3 from 9 to 18 wt.%, with Cr# ranging from 56 to 67. They have Mg# varying from 20 to 34 and XFe^{3+} from 0.16 to 0.34

(Table S2).

The $Kd_{Mg/Fe}^{Ol-Spl}$ for the samples from the Baixintan, Huangshannan, Luodong, and Tulaergen intrusions ranges from 3.7 to 16.0, 8.1 to 32.8, 6.4 to 14.5, and 10.3 to 12.9, respectively (Table S2).

3.3 *Dali picrite in the Emeishan LIP*

Olivine phenocrysts in the picrite have Fo contents ranging from 82 to 92. Spinel grains have Cr_2O_3 varying from 31 to 50 wt.% and Al_2O_3 from 13 to 29 wt.%, with Cr# ranging from 42 to 72. They have Mg# varying from 48 to 72 and XFe^{3+} from 0.05 to 0.10. The $Kd_{Mg/Fe}^{Ol-Spl}$ for the equilibrated olivine-spinel pairs is 4 to 6.

References cited

Bao Z., Chen L., Zong C., Yuan H., Chen K., and Dai, M. (2017) Development of pressed sulfide powder tablets for in situ sulfur and lead isotope measurement using LA-MC-ICP-MS. International Journal of Mass Spectrometry 421, 255-262.

Cao Y., Wang C.Y., and Wei B. (2019) Magma oxygen fugacity of Permian to Triassic Ni-Cu sulfide-bearing mafic-ultramafic intrusions in the central Asian orogenic belt, North China. Journal of Asian Earth Sciences 173, 250–262.

Chen L., Chen K., Bao Z., Liang P., Sun T., and Yuan H. (2017) Preparation of standards for in situ sulfur isotope measurement in sulfide using femtosecond laser ablation MC-ICP-MS. Journal of Analytical Atomic Spectrometry 32, 107-116.

Chung S.L., and Jahn B.M. (1995) Plume-lithosphere interaction in generation of the Emeishan flood basalts at the Permian-Triassic boundary. Geology 23, 889-892.

Davis F.A., Cottrell E., Birner S.K., Warren J.M., and Lopez O.G. (2017) Revisiting the electron microprobe method of spinel-olivine-orthopyroxene oxybarometry applied to spinel peridotites. American Mineralogist 102, 421–435.

Droop G.T.R. (1987) A general equation for estimating Fe^{3+} concentrations in ferro- magnesian silicates and oxides from microprobe analyses, using stoichiometric criteria. Mineralogical Magazine 51, 431–435.

Feng Y., Qian Z., Duan J., Xu G., Ren M., and Jiang C. (2018) Geochronological and geochemical study of the Baixintan magmatic Ni-Cu sulphide deposit: New implications for the exploration potential in the western part of the East Tianshan nickel belt (NW China). Ore Geology Reviews 95, 366–381.

Feng Y., Qian Z., Xu G., Duan J., Chen B., Sun T., Jiang C., and Ren M. (2017) Rock-forming mineral features of Permian mineralized mafic-ultramafic intrusions in East Tianshan Mountains and their implications for intrusion generation. Acta Petrological et Mineralogical 36, 519-534 (in Chinese with English abstract).

Hanski E., Kamenetsky V.S., Luo Z.Y., Xu Y.G., and Kuzmin D.V. (2010) Primitive magmas in the Emeishan Large Igneous Province, southwestern China and northern Vietnam. Lithos 119, 75–90.

Kamenetsky V.S., Chung S.-L., Kamenetsky M.B., and Kuzmin D.V. (2012) Picrites from the Emeishan large igneous province, SW China: a compositional continuum in primitive magmas and their respective mantle sources. Journal of Petrology 53, 2095-2113.

Liu Y., Hu Z., Gao S., Günther D., Xu J., Gao C., and Chen H. (2008) In situ analysis of major and trace elements of anhydrous minerals by LA-ICP-MS without applying an internal standard. Chemical Geology 257, 34–43.

Liu J., Xia Q.-K., Kuritani T., Hanski E., and Yu H.-R. (2017) Mantle hydration and the role of water in the generation of large igneous provinces. Nature Communication 8, 1824.

Mao Y., Qin K., Tang D., Feng H. and Xue S. (2016) Crustal contamination and sulfide immiscibility history of the Permian Huangshannan magmatic Ni-Cu sulfide deposit, East Tianshan, NW China. Journal of Asian Earth Sciences 129, 22–37.

Su B.X., Qin K.Z., Sakyi P.A., Li X.H., Yang Y.H., Sun H., Tang D.M., Liu P.P., Xiao Q.H., and Malaviarachchi S.P.K. (2011) U–Pb ages and Hf-O isotopes of zircons from Late Paleozoic mafic–ultramafic units in the southern Central Asian Orogenic Belt: tectonic implications and evidence for an Early-Permian mantle plume. Gondwana Research 20, 516–531.

Wang Y.L. (2011) Petrogenesis and mineralization of Heishan intrusion in Beishan area, Gansu. M.Sc. thesis, Chang'an University. (in Chinese with English abstract)

Wu Y., Ren Z., Handler M.R., Zhang L., and Qian S. (2018) Melt Diversity and Magmatic Evolution in the Dali Picrites, Emeishan Large Igneous Province. Journal of Geophysical Research: Solid Earth 123, 9635–9657.

Xie W., Song X., Deng Y., Wang Y., and Ba D. (2012) Geochemistry and petrogenetic implications of a Late Devonian mafic- ultramafic intrusion at the southern margin of the Central Asian Orogenic Belt. Lithos 144–145, 209–230.

Xu Y., Chung S., Jahn B., and Wu G. (2001) Petrologic and geochemical constraints on the petrogenesis of Permian- Triassic Emeishan flood basalts in southwestern China. Lithos 58, 145-168.

Yang S.H., Zhou M.F., Lightfoot P.C., Malpas J., Qu W.J., Zhou J.B., and Kong D.Y (2012) Selective crustal contamination and decoupling of lithophile and chalcophile element isotopes in sulfide-bearing mafic intrusions: an example from the Jingbulake intrusion, Xinjiang, NW China. Chemical Geology 302, 106–118.

Yuan H.L., Liu X., Chen L., Bao Z., Chen K., Zong C., Li X.C., and Qu W.J. (2018) Simultaneous measurement of sulfur and lead isotopes in sulfides using nanosecond laser ablation coupled with two multi-collector inductively coupled plasma mass spectrometers. Journal of Asian Earth Sciences 154, 386–396.

Zhao Y., Xue C., Liu S., Symons D.T.A., Zhao X., Yang Y., and Ke J. (2017) Copper isotope fractionation during sulfide-magma differentiation in the Tulaergen magmatic - Cu deposit, NW China. Lithos 286–287, 206–215.